New pigments based on carminic acid and smectites: A molecular investigation

David Guillermin, Theau Debroise, Pollyana Trigueiro, Laurence de Viguerie, Baptiste Rigaud, Fabrice Morlet-Savary, Sébastien Balme, Jean-Marc Janot, Frederik Tielens, Laurent Michot, et al.

New pigments based on carminic acid and smectites: a molecular investigation

David Guillermin[1], Theau Debroise[2], Pollyana Trigueiro[1], Laurence de Viguerie[1], Baptiste Rigaud[3], Fabrice Morlet-Savary[4], Sébastien Balme[5], Jean-Marc Janot[5], Frederik Tielens[2,6], Laurent Michot[7], Jacques Lalevee[4], Philippe Walter[1] and Maguy Jaber[1]*

Corresponding author: maguy.jaber@upmc.fr

[1]Sorbonne Université, Laboratoire d'Archéologie Moléculaire et Structurale, UMR 8220, 4 place Jussieu, F-75005 Paris, France
[2]Sorbonne Université, Laboratoire Chimie de la Matière Condensée, UMR 7574, 4 place Jussieu, F-75005 Paris, France
[3]Sorbonne Université, Institut des Matériaux de Paris Centre (FR2482), 4 place Jussieu, 75005 Paris, France
[4]Institut Européen des Membranes, UMR 5635, Université de Montpellier, ENSCM, CNRS, Place Eugène Bataillon, F-34095 Montpellier cedex 5, France
[5] Institut de Science des Matériaux de Mulhouse, UMR7361, CNRS, University of Haute Alsace, 15 rue Jean Starcky, 68057 Mulhouse Cedex, France
[6] General Chemistry (ALGC), Vrije Universiteit Brussel (Free University Brussels-VUB), Pleinlaan 2, 1050 Brussel, Belgium
[7] Sorbonne Université, Physicochimie des Electrolytes et Nanosystèmes interfaciaux, UMR 8220, 4 place Jussieu , F-75005 Paris, France

Abstract

Hybrid materials based on montmorillonite, a cationic polymer and carminic acid were prepared. The surface charge of montmorillonite was inversed thanks to the cationic polymer, polydiallyldimethylammonium chloride. Samples were characterized by a set of different techniques including Infrared (IR) and Nuclear Magnetic Resonance (NMR) spectroscopies to highlight the nature of the interactions between the organic and inorganic parts. The photo-stability of the samples was tested for different durations, and L*a*b* parameters were measured. It was possible to propose an approach for the degradation mechanism of the supported dye thanks to EPR (electron paramagnetic resonance) spectroscopy. The experimental data were in agreement with the theoretical periodic DFT calculations where a molecular scheme of the adsorption complex was proposed, and the importance of hydration on the stability of the adsorption complex highlighted.

Keywords: Montmorillonite, lake pigments, Carminic Acid, DFT, NMR, EPR

Introduction

Natural organic dyes and pigments are key components of cultural heritage artifacts and understanding their durability is a crucial issue. These two types of materials have distinct features. Indeed dyes are soluble in the medium in which they are present [1]. Furthermore, dyes are able to absorb light in the visible range of electromagnetic radiation (400–700 nm), bear a chromophore group, and can also possess an auxochrome group. In contrast, pigments are generally inorganic and insoluble [2] and the mixture between a dye and an inorganic material or metallic cation such as aluminum or tin can therefore be used as a pigment. The latter are known to be more sensitive to fading. The weak photo-resistance of the red lake pigments used in paintings by the Impressionists has been reported. A very good illustration is the painting by Pierre Auguste Renoir: "Madame Léon Clapisson", where the red colors have faded as a result of the levels of light and humidity in the museum[3].

The approach based on the preparation of hybrid materials where dyes are inserted into inorganic matrices, is currently widely employed in numerous applications dealing with pigments such as for instance solar cells [4], laser applications or art. Various strategies have been used for obtaining resistant, chemically stable pigments. Among them, sol-gel techniques and adsorption of organic dyes in inorganic matrixes have been widely studied [5-10]. As far as this latter approach is concerned, numerous studies have reported organic dyes stability enhancement through complexation with swelling clay minerals [11-17], an approach that follows the famous case of Maya Blue, in which blue dyes are adsorbed onto fibrous sepiolite or palygorskite [18]. The use of clay minerals appears particularly attractive as these materials do not absorb light in the visible wavelength region, are environmentally friendly, abundant and rather cheap.

Among the large family of red dyes molecules, carminic acid is an organic dye ,widely used in the cosmetic industry and as a food colorant [19].Chemically speaking, it is a hydroxyanthraquinone with a lateral chain of C- glycosyl and only one position free on the aromatic nucleus. Its pKa values were reported to be pKa1 = 2.81 ± 0.09; pKa2 = 5.43 ± 0.04; pKa3 = 8.10 ± 0.03[20]. For pH values higher than 3, carminic acid is therefore negatively charged. As a consequence, the direct preparation of swelling clays/carminic acids hybrids cannot be achieved, as these minerals bear a permanent negative charge, which will lead to repulsive interactions upon mixing carminic acid with non-treated swelling clays [8]. The preparation of clay/carminic acids hybrid materials therefore requires a pre-treatment stage to change the surface charge of the clays.

Various strategies can be employed to reverse the surface charge of clay minerals. The first one is to adsorb excess cationic surfactants[21], such as hexadecyltrimethylammonium or cetylpyridium chloride. These molecules bear a positively charged hydrophilic head (usually through the presence of an ammonium functional group) and a neutral hydrophobic tail. The head can be adsorbed onto the negatively charged surface to form the first layer of the surfactant, and additional surfactant adsorption will then yield a positive surface charge[21]. Another solution is to change the external surface using silane molecules such as aminopropyltriethoxysilane [22, 23] that is positively charged in acidic aqueous solutions. It is also possible to adsorb cationic polymers such as PDADMAC (Poly (diallyldimethylammonium chloride) at the clay surface. In such conditions, stable clay suspensions [20] in which particles bear a net positive charge [24-26] can be obtained. For this reason, polycation-clay systems have recently been the object of renewed attention as potential nano-composites for surface applications[24-26].

In the present paper, we apply this latter method for preparing montmorillonite/carminic acids pigments. The pigments obtained in this way are characterized in depth using numerous

experimental techniques including XRD, thermal analysis, IR, ^{13}C solid state NMR and EPR (Electron Paramagnetic Resonance) spectroscopies and zeta potential measurements. The conformation and geometry of both cationic polymer and dye in the hybrid materials are further analyzed by density functional theory (DFT). Finally, extensive spectro-photocolorimetric analyses are carried out to investigate the influence of dye-montmorillonite interactions on the stability/degradation of the resulting hybrids under light and in the presence of different solvents.

Experimental part

A. Reagents:

Carminic acid (90%, wt) and Poly(diallyldimethylammonium chloride) solution in water (20%, wt), were purchased from Sigma-Aldrich.

B. Montmorillonite synthesis

Montmorillonite synthesis was carried out using classical procedures [27]. Hydrofluoric acid (HF, 40% w/w; Fluka), sodium acetate ($NaCOOCH_3$, 99%; Fluka), magnesium acetate [$Mg(COOCH_3)_2.4H_2O$, 99%; Fluka], boehmite (Al_2O_3, 74%, Pural SB1; Condea), and silica (SiO_2, 99.5%, Aerosil 130; Degussa) were mixed for preparing an initial hydrogel with the following chemical composition: $1SiO_2$: $0.2Al_2O_3$: 0.1MgO: $0.05Na_2O$: 0.05HF: $96H_2O$. This hydrogel was matured during 4 h at room temperature before being introduced into a PTFE-lined stainless steel autoclave where it was heated at 473 K during 96 h. After cooling down to room temperature, the solid was recovered by centrifugation, washed thoroughly with distilled water and dried at 333 K for 12 h. The ideal formula per half unit cell of the montmorillonite thus synthesized can be written as $Na_{0.4}[(Si_4)(Al_{1.6}Mg_{0.4}\square)O_{10}(OH,F)_2]$, where $\square$ refers to the vacancies in the octahedral sheets, yielding a cationic exchange capacity of 1.09 $meq.g^{-1}$ [27, 28].

C. Surface modification of the different clay minerals

A wet impregnation procedure was used for adsorbing Poly(diallyldimethylammonium chloride) on montmorillonite. In a typical preparation, 40 mg of a 20 wt% PDADMA solution were mixed with 100 mg of dry sodic clay. Water was then added to obtain a homogeneous suspension. Samples were dried overnight at 333K. The amount of cationic polymer was varied and samples will be referred to as "x/y-Mt" where "x/y" is a molar ratio with "x" the negative charges hold by the clay (Mt) and "y" the positive charges brought by the cationic polymer (CP). The following ratios were used: 1/1, 2/3, 1/2 and 1/3.

D. Adsorption of carminic acid

10 % of carminic acid with a concentration of 5mg/mL in distilled water was added to Na-Mt at an average working pH of 6 as already reported in the literature[29-31]. An excess of carminic acid induces a strong release in solution. The suspension was stirred for 4 h, the time request to reach the equilibrium[8]. After centrifugation, the resulting solids were dried at 333K overnight. Presence of carminic acid is indicated by the prefix CA in sample names e.g.: CA_1/2_Mt.

E. Desorption experiments

Desorption experiments were performed by dispersing 10 mg of selected samples in a 2 mL conical flask with 1 mL of solvent and shaking at room temperature for 1 h. The desorption of CA from the hybrid material after centrifugation was measured by absorption at λ = 495 nm since carminic acid has its maximum of absorption at the later wavelength.

F. Photo-fading

The evolution of samples under visible light was followed by placing them under a SL164 LED from Advanced Illumination Company during 400 hours. As this lamp provides a flux of 50 Klux per hour, such a procedure can also provide information about the long time

evolution of the samples. Indeed, the total dose after 400 hours of illumination is equivalent to a 30 years illumination under a classical lamp with a flux of 200 lux per hour.

G. Characterization

X-Ray powder diffraction (XRD) was carried out with a Bruker D8 Advance diffractometer using the Cu Kα radiation (wavelength λ = 1.5404 Å). XRD patterns were recorded between 5° and 70° with a step size of 0.05°. Thermogravimetric analysis (TGA) of the samples was performed on a TA Instruments – Waters LLC, SDT Q600 analyzer with a heating rate of 5 °C.min^{-1} under dry air flow (100 mL.min^{-1}). Transmission Electron Microscopy (TEM) measurements of the samples were performed using a JEOL100CX microscope. Samples in the form of bulk powders were suspended in ethanol and then deposited on specific grids (400 mesh copper grids covered with an ultrathin carbon membrane of 2–3 nm thickness).

Zeta potential measurement were performed at controlled temperature, fixed ionic strength ($NaNO_3$ solution at 1.10^{-4} mol.L^{-1}) and at 5<pH<5.5, using a Malvern Zetasizer nanoZS device.

Spectrophotocolorimetry was performed using Ocean Optics halogen light source HL-2000-FHSA as incident light beam and Ocean Optics USB4000 detector with Ocean Optics QP400-1-UV-VIS glass fibers for acquisition from 350 to 1050 nm on pressed pellets samples. Data were collected with OceanView 1.5.0 software in color measurement mode, and an average of 100 scans was performed for each measurement to obtain the optimum signal.

ATR/FTIR spectra were recorded at room temperature with a Cary 630 Agilent spectrometer. For each measurement, three spectra were recorded as an accumulation of 32 scans, with a spectral resolution of 4 cm^{-1}.

The ^{13}C Cross-Polarization spectra were acquired with a MAS rate of 14 kHz, a ramp-CP contact time of 1 ms and a 1 s recycle delay and with a ^{1}H decoupling spinal. Over an

acquisition time of 40 ms, the number of scans to obtain the spectra depends on the S/N obtained for each sample. Spectra were processed with a zero-filling factor of 2 and with an exponential decay corresponding to a 25 Hz line broadening in the transformed spectra. Only spectra with the same line broadening are directly compared.

Epifluorescence microscopy was performed on a LEICA MD 6500 microscope. Time-resolved fluorescence spectroscopy data were obtained by the time-correlated single-photon counting technique using a lab-made device previously described [32, 33]. For the analysis, the fluorescence decay law at the magic angle $I_M(t)$ and the anisotropy decay law $r(t)$ were analyzed as a sum of exponentials :

$$I_M(t) = \frac{1}{3}\sum_{i=1}^{n} \alpha_i \, e^{-t/\tau_i} \qquad \text{(eq 1)}$$

$$r(t) = \sum_{j=1}^{n} r_j \, e^{-t/\phi_j} \qquad \text{(eq 2)}$$

With τ_i the fluorescence lifetime, α_i the pre-exponential factor related to the contribution of each lifetime of component *i*, r_j the anisotropy of a component *j* for a correlation time ϕ_j.

The anisotropy decay, r(t) is related to the decays collected with vertical, $I_V(t)$, and horizontal, $I_H(t)$, polarization, the excitation being vertical:

$$I_V(t) = I_M(t)\{1 + 2r(t)\} \qquad \text{(eq 3)}$$

$$I_H(t) = I_M(t)\{1 - r(t)\} \qquad \text{(eq 4) or } r(t) = \frac{I_V(t) - I_H(t)}{I_V(t) + 2I_H(t)} \qquad \text{(eq 5)}$$

Fluorescence lifetimes were calculated from data collected at the magic angle by iterative adjustment after convolution of a pump profile (scattered light) with a sum of exponentials as described previously.

EPR experiments were carried out at room temperature and in aerated medium using an X-Band spectrometer (EMX plus Bruker). Radicals can be observed either directly or by the spin trapping technique (ESR-ST) in the presence of phenyl N-tert-butyl nitrone (PBN, 3) according to scheme S1. The procedure has been described in detail elsewhere [1,2]. PBN was selected as spin trap agent due to its rather good stability upon light irradiation. ESR spectra simulations were carried out with the WINSIM software, extracting the hyperfine coupling constants (hfc) a_N and a_H from the ESR simulated spectra. Values are related to the trapped (or adduct) radical R° by the PBN moiety.

The reduction potential (Ered vs. SCE) and oxidation potential (Eox vs. SCE) of the studied compound was determined by cyclic voltammetry (Voltalab PST006) in acetonitrile solution containing tetrabutylammonium hexafluorophosphate (Aldrich) as the supporting electrolyte. A platinum electrode was used as a working electrode and a saturated calomel electrode (SCE) was used as a reference electrode.

H. Computational Details

All geometry (atom positions + unit cell parameters) optimizations were performed using an ab initio plane-wave pseudopotential approach as implemented in VASP[34, 35]. The PBE functional [36, 37] was chosen to perform periodic DFT calculations with an accuracy on the overall convergence tested elsewhere [38-40]. The valence electrons are treated explicitly and their interactions with the ionic cores are described by the Projector Augmented-Wave method (PAW) [36, 37], which allows using a low energy cut off equal to 500 eV for the plane-wave basis. A 3 × 3 × 1 Monkhorst-Pack mesh of k-Points is used in the Brillouin-zone integration. Partial occupancies of the wave functions are determined using the tetrahedron method with Blöchl corrections[41].

Since our system involves interacting organic molecules, the influence of introducing dispersion forces was investigated by using the Grimme[42] D2 method as implemented in VASP 5.4. vdW-DF was used by means of the optPBE functional[43].

Bulk Models

The bulk model of Mt was built in order to be as close as possible to the synthetized MT while remaining calculable by DFT. The periodic super cell used in the calculations had the raw formula: $\mathbf{Al_{18}Mg_6Si_{48}O_{120}Na_6(OH)_{24}}$. The super cell corresponds to a formula per half unit cell of $\mathbf{Na_{0.5}[(Al_{1.5}Mg_{0.5})Si_4O_{10}(OH)_2]}$. This compares well with the experimental formula $\mathbf{Na_{0.4}[\ (Al_{1.6}Mg_{0.4})Si_4O_{10}(OH)_2]}$. The Na^+ cations compensate for the negative charge of the material. They can be replaced by the cationic polymer PDADMAC. One monomer of PDADMAC is charged +1. In the model (See Figure 1), 6 monomers PDADMAC are needed to replace 6 Na^+.

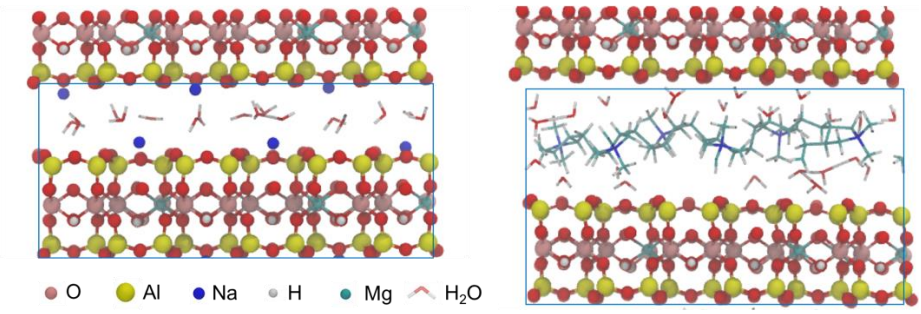

Figure 1: Two bulk models of Mt with and without the cationic polymer

As shown in Figure 1, a monolayer of water molecules was considered in the interlayer space of Mt. The number of water molecules was chosen in order to be consistent with TG-DTA experiments. For one periodic super cell, 16 water molecules were added, corresponding to 1.33 water molecules per half unit cell. Finally, the corresponding raw formula per half unit cell is $\mathbf{Na_{0.5}[(Al_{1.5}Mg_{0.5})Si_4O_{10}(OH)_2]1.33H_2O}$.

Adsorption

Models

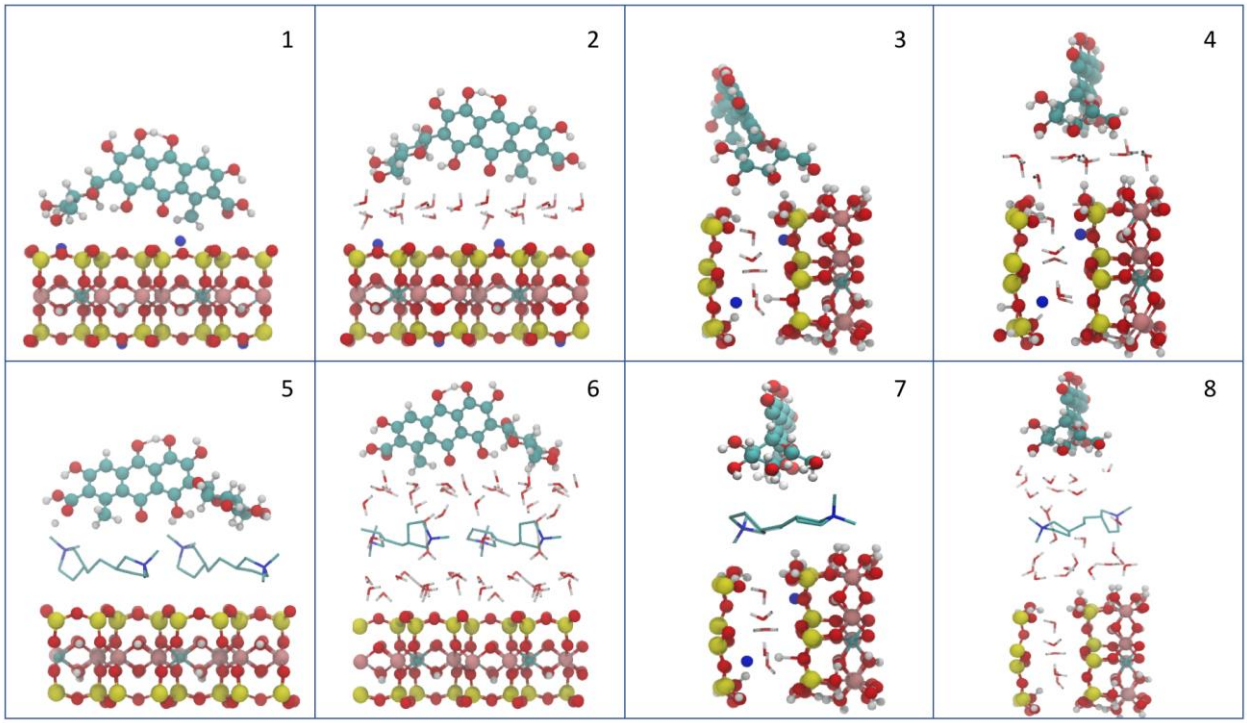

Figure 2: Eight adsorption models of CA on dry MT 001 (left) and 100 (right) surfaces

The considered Mt periodic cell formula is $\mathbf{Na_4[(Al_{12}Mg_4)Si_{32}O_{80}(OH)_{16}]}$. In this study, the PDADMAC was modeled by two dimers instead of one polymer and the CH_3 groups were removed for the sake of unit cell size consistency. The presence of the PDADMAC's methyl groups would not have allowed reasonable calculations in an optimum time. The (001) surface model corresponds to the same model as the bulk but with a larger interlayer distance. This leads to negligible interactions between Mt layers. For the (100) surface the Mt bulk was cut perpendicularly to a layer. H and O atoms were added in order to neutralize surface charge. At the end, OH groups are exposed on the surface. Each of the two surfaces was calculated in dry or hydrated conditions, with or without PDADMAC, leading to a total of 8 surface models.

These surface models are presented with CA above in Figure 2.

The adsorption energy of CA on a surface is calculated as the difference between the total energy of the surface with adsorbed CA and the sum of the total energy of the bare surface and the total energy of isolated CA as follows:

$$E_{ads} = E(surface + CA) - E(surface) - E(CA) \qquad \text{(eq. 6)}$$

Results and discussion

X-ray diffraction

XRD pattern of the initial montmorillonite exhibit (hkl) bands typical of smectites (Figure 3).***[44]***

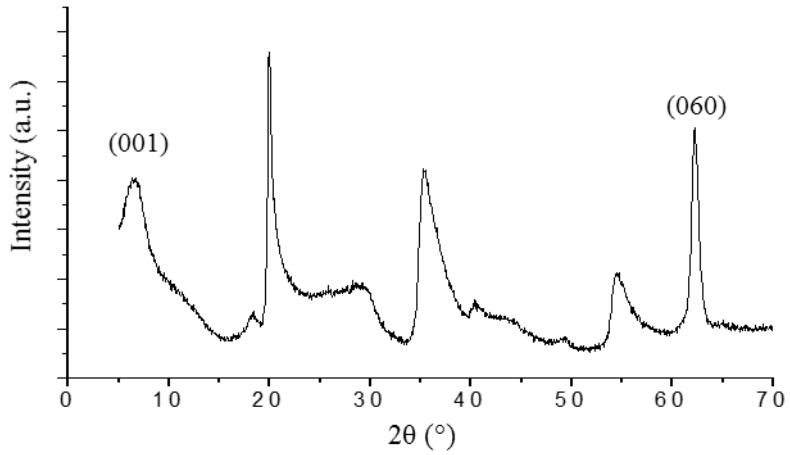

Figure 3: X-ray diffraction pattern of the Na^+- Mt

The (001) reflection corresponds to an inter-reticular distance of 1.26 nm that can be assigned to "one" water layer for montmorillonite. The d_{060} value of 0.149 nm is consistent with the dioctahedral character of the layers (occupation of 2/3 of the octahedral cavities by trivalent elements).

After mixing with the cationic polymer, the d_{001} value reaches 1.47 nm whatever the amount of organic matter, indicating that the polymer is probably intercalated in the interlayer space. The addition of carminic acid to the composite "cationic polymer_Mt" does not lead to

considerable changes in the XRD pattern except for a narrowing of the (001) reflection (Figure 4).

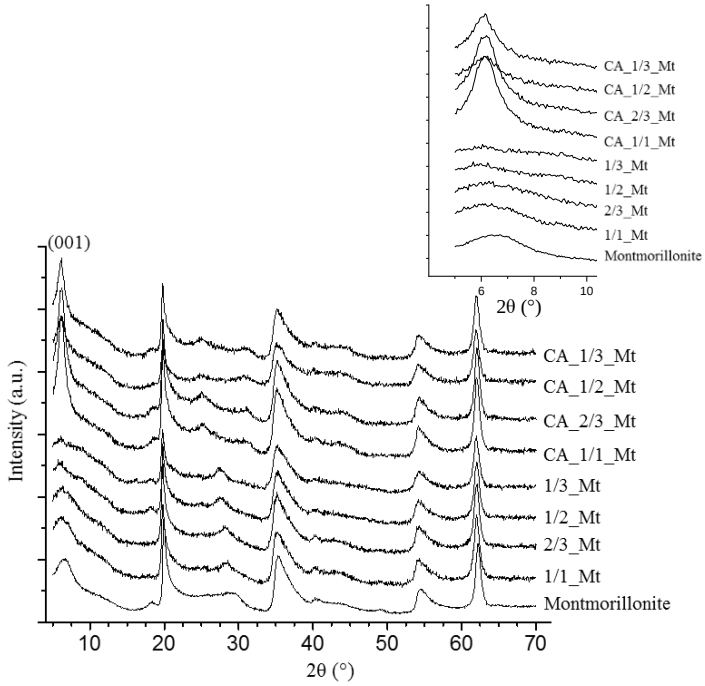

Figure 4: XRD patterns of raw Mt and all hybrid materials, in insert a zoom on the (001) reflection.

Such narrowing could be due to a rearrangement of polymer moieties in the interlayer space. Indeed, the adsorption of the cationic polymer was performed by wet impregnation without any washing procedure whereas the dyeing procedure was followed by a washing step that likely removed the sodium cations exchanged by the cationic polymer in the interlayer space. An additional reflection is observed for these samples around 25° in 2θ and is attributed to the (004) plan, attesting a better organization of the layers along the c-axis.

Transmission Electron Microscopy

In order to investigate more precisely polymer intercalation in the interlayer space of Mt, TEM experiments were conducted. The micrograph corresponding to raw Mt exhibits layers with a $d_{(001)}$ value of ~ 1.2 nm. As regards the CA-CP-Mt micrographs (Figure 5), they exhibit stacked layers with a $d_{(001)}$ spacing of ~1.30 nm. Such a value is significantly higher than the

value obtained for the starting montmorillonite and is also rather high considering the fact that the microscope operates under vacuum. It then strongly suggests that cationic polymer molecules are present in the interlayer space of montmorillonite after the impregnation procedure.

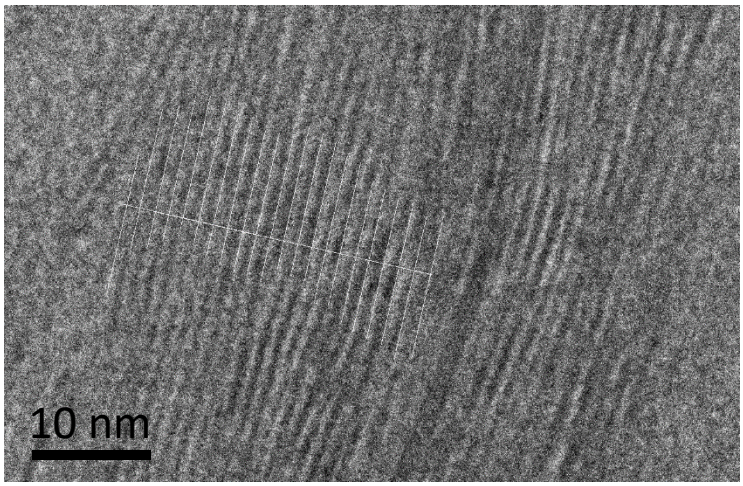

Figure 5: TEM image of CA-CP-Mt composites oriented along C-axis.

DFT Calculations

The interlayer distance was calculated as the distance between the center of an oxygen atom from the top layer and the center of an oxygen atom from the bottom layer minus one oxygen van der Waals radii. If the cationic polymer is in the interlayer space of bulk Mt, an equilibrium interlayer distance of 7.6 Å was calculated. This is to be compared to the value of 3.6 Å that was calculated for the same model with Na^+ ions as interlayer cations. A d_{001} of 1.427 nm should then be obtained for polymer-intercalated montmorillonite, which concurs with XRD results.

Table 1: interlayer distances of Mt bulk with Na^+ cations or cationic polymer as counter ions

Interlayer ions	**Na^+**	**PDADMAC**
Interlayer	3.6 Å	7.6 Å

Theoretical Distance		

Table 2: Adsorption Energies of Carminic Acid (CA) on Mt 001 and 100 Surfaces (kJ/mol). The numbers in the table correspond to the model numbers in Figure 2.

Model	001 surface	100 surface
Mt CA	**1 :** -7.9	**3 :** -24.0
Mt-polymer CA	**5 :** +3.9	**7 :** +3.1
MT CA hydrated	**2 :** -58.9	**4 :** -60.6
MT-polymer CA hydrated	**6 :** -57.2	**8 :** -59.7

No stabilization of CA on dry Mt surfaces (001) and (100) was observed. On the contrary, a consistent stabilization was observed on the hydrated surfaces. This highlights the role of water in such a composite. It can act as a glue to fix molecules at the surfaces of Mt, as has been observed and confirmed in the case of silica[45-48] e.g. This behavior is due to the capacity of water molecules to form a flexible network of hydrogen bonds between the adsorbate and the substrate. Interestingly, no significant difference in adsorption energy was found between (001) and (100) surfaces of Mt.

Thermogravimetric Analysis

The amount of adsorbed organic matter in the composite materials was obtained by thermal analysis. The DTG curves corresponding to the raw materials and to all the cationic polymer/carminic acid composites are shown in Figure 6a and b. For raw Mt, water loss occurs at low temperature (< 200°C) whereas dehydroxylation corresponding to a weight loss of 5.6% is observed at high temperature around 650°C. For pure cationic polymer, a first endothermal signal assigned to water loss of is observed below 200°C. Organic matter degradation occurs in the range 230-620°C and is accompanied by an exothermal signal

observed by DTA (not shown). Carminic acid displays a similar behavior with a water weight loss occurring before 130°C and the oxidation of the organic part between 130°C and 530°C. The DTG curves of CP-Mt composites can be separated in three regions. In the 30°C-170°C range, a large weight loss associated with an endotherm corresponds to the elimination of physisorbed water (including interlayer water for the smectite supports). The corresponding amounts in this step are 6, 14.1, 10.1, 5.9 and 5.9 % for Mt, 1/1_Mt, 2/3_Mt, 1/2_Mt and 1/3_Mt, respectively. The region 200-730°C corresponds to the decomposition of the cationic polymer an accounts for weight losses of 9.6, 13.7, 16.3 and 30.3 % 1/1_Mt, 2/3_Mt, 1/2_Mt and 1/3_Mt, respectively. For the highest amount of cationic polymer, the presence of sharp peaks around 330-400°C on the DTG curve suggest that some polymer remains free. Assuming that dehydroxylation also occurs in the composites and still corresponds to a 5.6% wt loss, and assuming that all weight losses for temperatures higher than 170° are due to elimination of organic material, the total amount of organic matter calculated from the total weight loss between 170 and 730 °C is 19.7, 23.1, 27.6 and 28.6 % for CA_1/1_Mt, CA_2/3_Mt, CA_1/2_Mt and CA_1/3_Mt, respectively. Comparing lost amounts between CP-Mt composites and CA-CP-Mt composites suggests that for the highest amount of cationic polymer, the free part of cationic polymer is somehow replaced by adsorbed carminic.

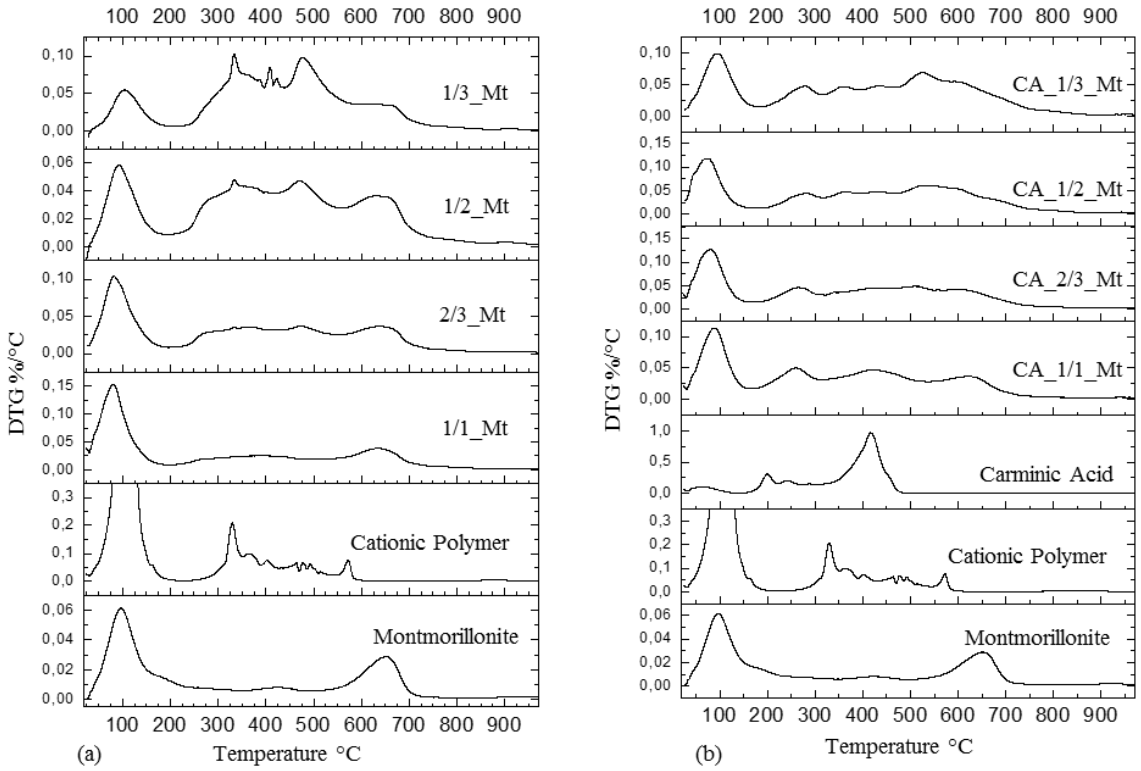

Figure 6: DTG curves of (a) raw Mt and its hybrid derivatives with the cationic polymer and (b) raw Mt and the composites based on CA-CP-Mt.

Zeta Potential

As expected, raw montmorillonite, displays a negative surface charge (-40 mV). After adsorption of the cationic polymer, the measured zeta potential evolves with the amount of fixed polycation. For a montmorillonite/polymer ratio of 1/1 the surface charge is still negative (-25mV), which suggests that the exchange between sodium cations and polycations is not complete. The point of zero charge is reached for a ratio of 2/3 and charge reversal starts occurring for a theoretical ratio of 1/2.

Infrared spectroscopy

The FTIR spectra of raw montmorillonite is displayed in figure 7: a band at 3635 cm-1 corresponding to structural OH groups is observed. The presence of hydration water can be inferred from the existence of a broad multicomponent band between ≈ 3500 -3000 cm^{-1}, assigned to OH stretching vibrations (νO-H) and a signal at 1630-1640 cm^{-1} assigned to the

δH-O-H band. In the low-energy region, bands characteristic of the vibrations of the sheets are present: one broad band with a maximum at 1045-1050 cm^{-1} and shoulders at 1015-1017 and 1080 cm^{-1}, assigned to Si-O stretching and Si-O-Si bending vibrations of the tetrahedral sheet together with a band at 918 cm^{-1} associated with (Al, Al)-OH vibrations in the octahedral sheet.

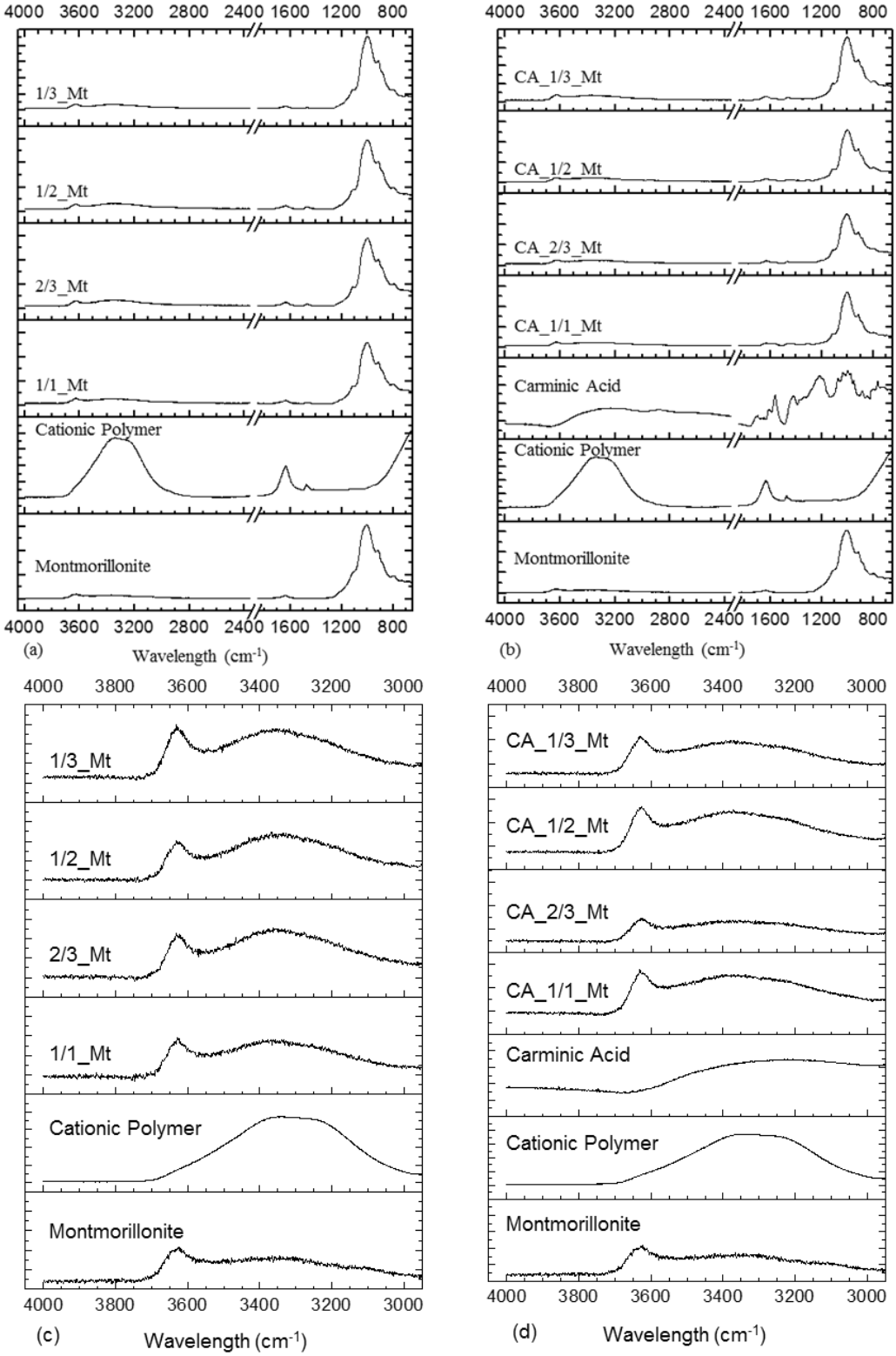

Figure 7: IR spectra of the (a) raw Mt and its hybrid derivatives with the cationic polymer, (b) raw Mt with the composites based on CA-CP-Mt and (c) and (d) respectively zooms of (a) and (b) in the 4000-3000 cm^{-1} water region.

The IR spectrum of the cationic polymer displays a broad signal in the region 3100-3600 cm^{-1}, where bands assigned to the –OH (water) and to protonated amine are overlapping[49]. The presence of a band at 1465 cm^{-1} indicates a long carbon chain with a high degree of regularity for the linear backbone structure.

The spectrum corresponding to carminic acid displays specific features. Some of them are linked to aromatic functions such as C=C stretching vibrations (1560 cm^{-1}) and –CH deformational vibrations (660 cm^{-1}). In addition, the spectrum exhibits a clear signal at ~890 cm^{-1} assigned to bending vibrations of OH groups from carboxyl group and bands in the region 1200-1250 cm^{-1} assigned to catechol functions [50-52]. The IR spectra of the montmorillonite/cationic polymer composites do not show any specific signals that could indicate particular interaction between compounds.

Nuclear Magnetic Resonance

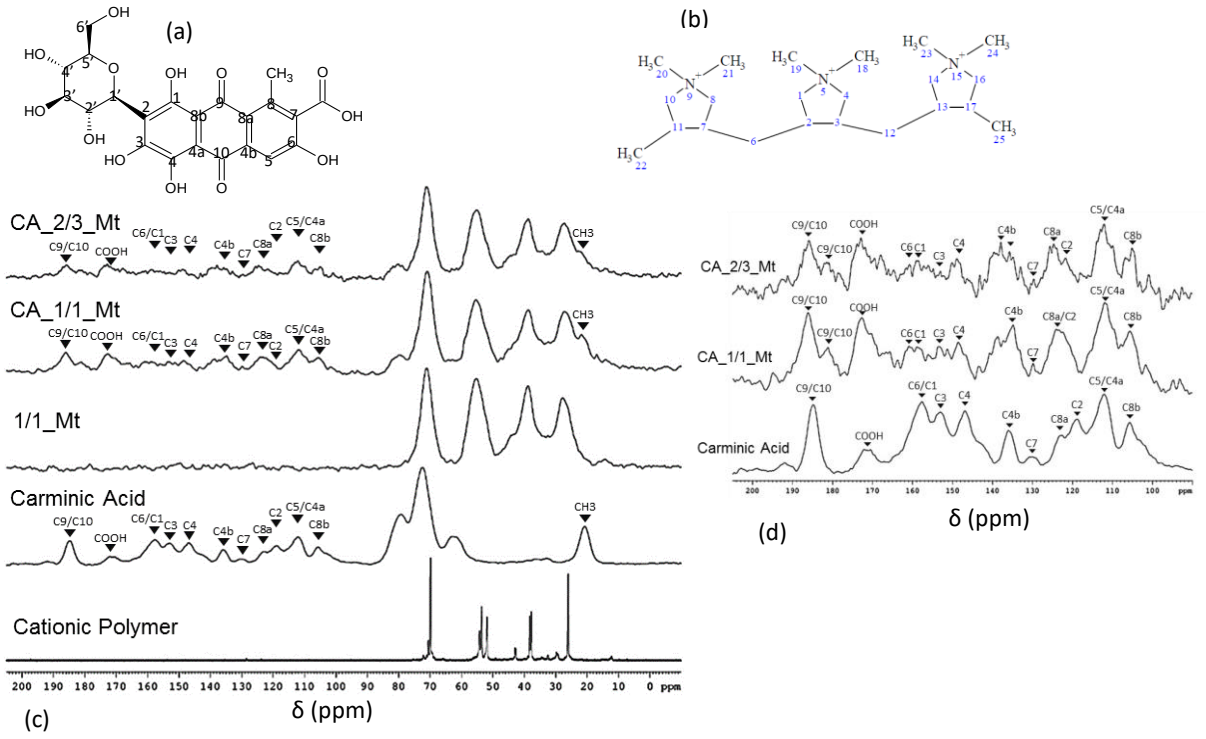

Figure 8: (a) carminic acid structure (b) Cationic polymer structure (c) NMR spectra of hybrid materials, cationic polymer and carminic acid and in insert (d) zoom in the 100-200 ppm region.

^{13}C CP-MAS NMR spectra of some selected samples are presented in Figure 8. The ^{13}C NMR spectrum of carminic acid displays resonances over a wide range of chemical shifts. The peak at 20.8 ppm is assigned to the methyl group linked to the C8. The region between 60 and 80 ppm corresponds to the sugar part of the dye molecule. The numerous peaks at higher chemical shifts correspond to the various C atoms of carminic acid whereas the peak at 172 ppm is assigned to carboxylate moieties and that at 185 ppm to ketones functions.

The spectrum of the cationic polymer displays several peaks in the region of 10 to 75 ppm. The peaks in the region 50-57 ppm are related to C22, C23, C25. The signals of the carbons bearing the nitrogen (in the cationic polymer) are located in the region 66-77 ppm.

The spectrum of 1-1 CP-Mt composite displays all the peaks previously assigned to the cationic polymer. Still, no direct comparison can be done since the pure polymer is liquid whereas the composite is solid.

Spectra of CA-CP-Mt composites display two series of peaks: that corresponding to the dye molecule and that to the cationic polymer. These latter signals are not affected by the presence of the CA, which confirms that polymer intercalation in montmorillonite is not modified in the presence of CA. In contrast, several changes can be observed in the region assigned to the organic dye and are highlighted in Figure 8d: a splitting of the peak assigned to the ketone functions is observed resulting in peaks at 186 and 181 ppm. In the range corresponding to carboxylic acid, additional peaks appear at 168.8 and 166 ppm. The signals assigned to the carbons bearing the –OH (C1, C3, C4 and C6) are strongly affected in the region 147-158

ppm. Finally, the peak at 72.6 ppm assigned to the OH bearing carbon is shifted to 71.3 ppm where it overlaps the signal assigned to the nitrogen bearing carbon in the cationic polymer.

Fluorescence imaging and time resolved fluorescence

In a previous work we showed that the fluorescence lifetime of carminic acid was strongly dependent on the nature of the exchangeable cation of Mt[44, 53]. The fluorescence decay of carminic acid was recorded under an excitation wavelength of 540 nm and at different wavelengths from 560 nm to 670 nm by 10 nm step. In water, carminic acid has an average fluorescence lifetime of 0.2 ns that can be decomposed into 3 components 0.09 ns, 0.46 ns and 1.33 ns. When adsorbed on cationic polymer-Mt, the average fluorescence lifetime is longer (0.54 ns). The anisotropy functions that are directly connected to rotational diffusion coefficient due to Brownian motion yield a long correlation time (~50 ns) much longer that in solution (≈ 0.3 ns)[54]. This long correlation time can be assigned to the rotation of carminic acid loaded on clay, and the lack of any short correlation time confirms that carminic acid is not released from the surface, which concurs with fluorescence microcopy results that show that dye is only located on clay particles.

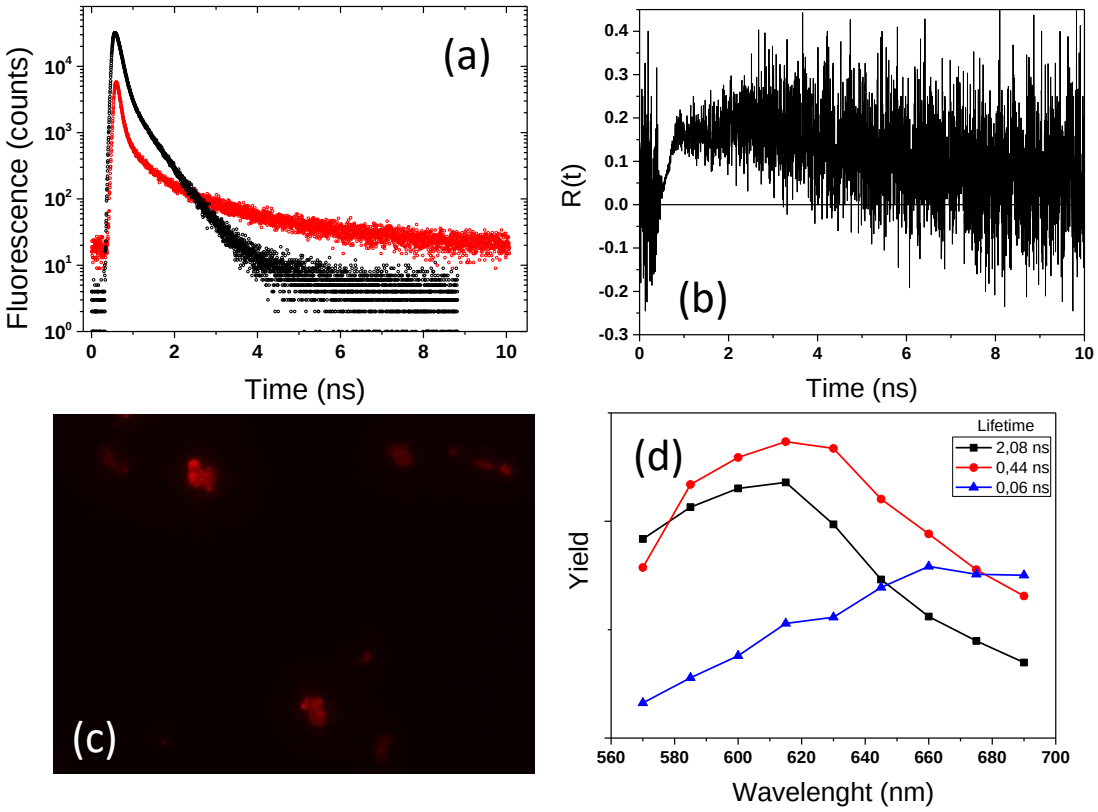

Figure 9: Fluorescence analysis (a) fluorescent decay of Carminic acid loaded on polymer-Mt (red) and free in water (black) (b) anisotropy function of Carminic acid loaded on polymer-Mt (c) epifluorescent imaging (d) spectra of each lifetime of Carminic acid loaded on polymer-Mt.

To deepen our investigation, the fluorescence decay of carminic acid loaded on cationic polymer-clay was recorded at different wavelength from 560 to 700 nm. Four components are required ~~(~~4 lifetimes~~)~~ for a proper analysis of decays. The shorter one ~0.01 ns could be assigned to a contribution of scattered light. This is however unlikely as a double monochromator was used in the experiments. The three other lifetimes measured are 0.06 ns, 0.44 ns and 2.08 ns. This latter time is significantly higher than that of carminic acid in solution, which again confirms the interaction between dye and solid.

Desorption test

Desorption tests for samples containing CA were carried out in different solvents: distilled water at pH 6, ethanol and ethylene glycol. No release of the dye was ever observed and the results were confirmed by resolved time fluorescence.

Spectrophotocolorimetry

To follow the ageing and fading of samples, pellets 5mm in diameter were pressed to obtain a flat surface allowing an easy and reproducible acquisition of the spectrum in visible light.

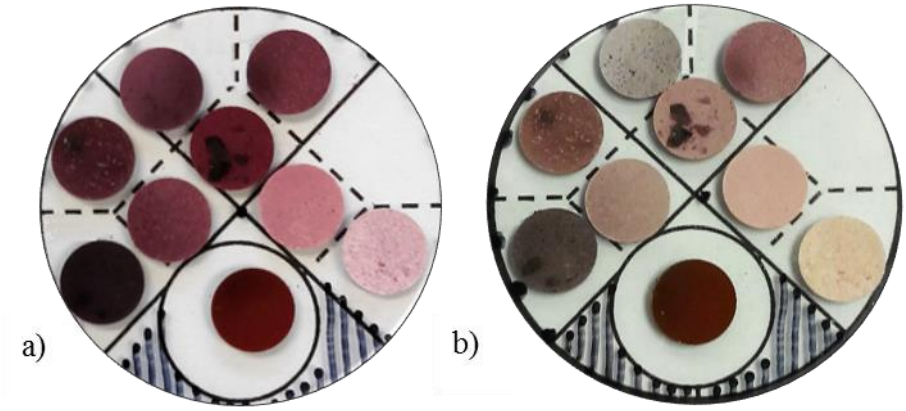

Figure 10: Color of the samples before exposition a) and after 400h under light b)

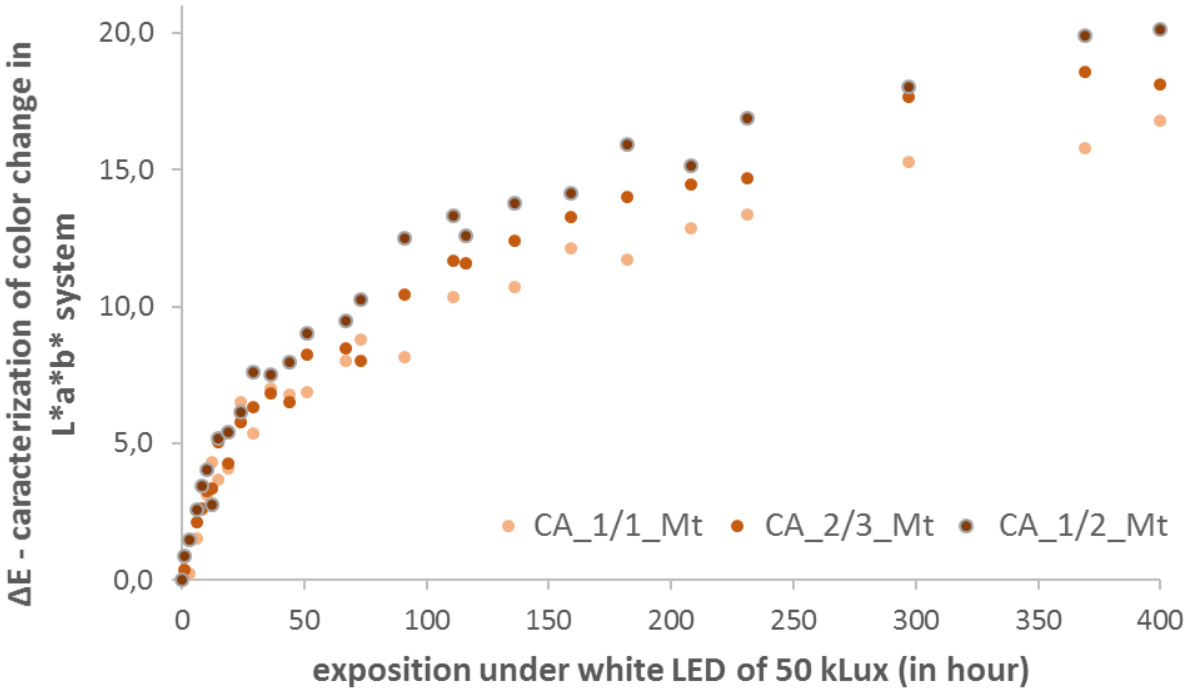

Figure 11: Ageing of pigments followed by color change observations over the 400h exposition under light.

The different dyed samples were submitted to ageing under light. Different measurements of the parameters L*a*b* were performed at different light irradiation time. Fading is observed in the first hours of irradiation for the Mt-carminic acid solid (blank). At longer times, all curves are close to each other. The presence of the cationic polymer in the composite CP-CA-Mt then does not seem to affect the photostability of the samples even if it prevents the dye from being released in different solvents.

Electron Paramagnetic Resonance

To follow the degradation of the pigment, samples with different ageing were prepared. CA_1/2_Mt – New were synthetized just before the EPR experiment, while others were placed under ambient light condition during 6 and 12 months, respectively. EPR results expressed in normalized intensities are shown in Figure 12.

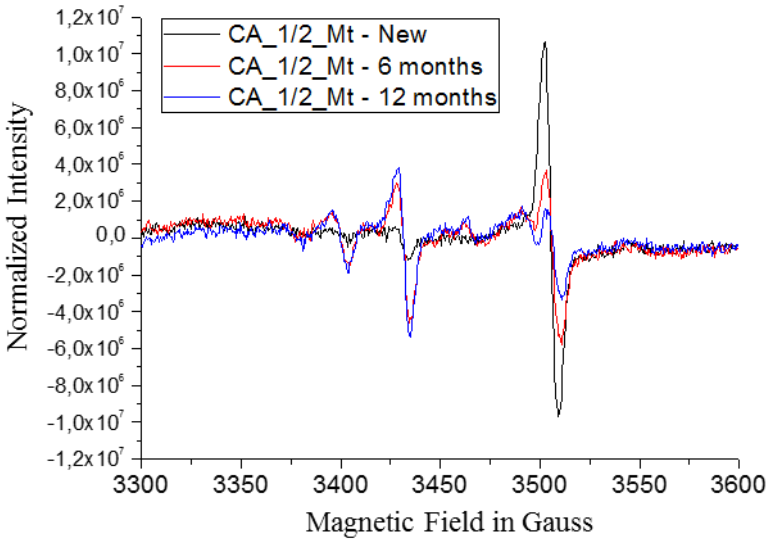

Figure 12: EPR on samples with long time exposure to ambient light

Three main contributions can be observed at 3400 G, 3430 G and 3500 G. They all correspond to organic radicals and can be assigned to carminic acid, as samples with cationic polymer only do not exhibit any EPR signal. Fresh pigment does not display any clear contribution at 3400 G or 3430 G and a strong signal at 3500 G that is much higher than for

aged pigments. In contrast, both aged samples display a weaker contribution at 3500G and stronger signals at 3400 and 3430 G, longer aging resulting in decreasing signals at 3500G and increasing ones at both 3400 and 3430 G. The ageing process then appears to occur in subsequent steps, with a rapid formation of radicals at 3500 G that then evolve to form at 3400 G and 3430 G.

In order to see if intense light could drive a fast radical production, EPR experiments were performed after some focused ageing of the pigments using a laser beam. Two types of laser were used: a green one, as it is the main absorbed color from the red carminic acid dye (see Figure 13), and an UV one, as UV illumination is commonly used for forming radicals on organic compounds. No change could be observed at either 3400 G or 3430 G, but the 3500 G radicals were clearly sensitive to the light beam, 7 minutes of laser illumination leading to increased signals at 3500 G (see Figure 14).

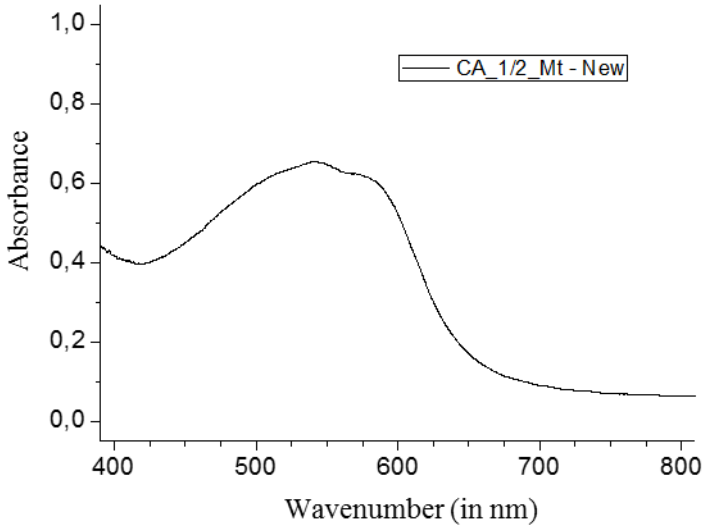

Figure 13: Pigment Absorbance in the visible light range

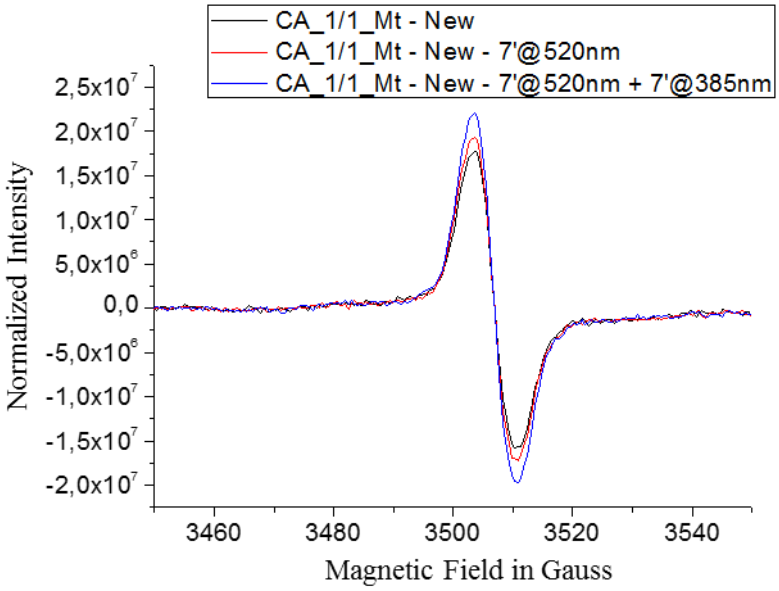

Figure 14: EPR on samples with short time exposure to focused light

Finally, the "g" values corresponding to the 3 radicals observed by EPR spectroscopy can be calculated.

g_1 = 2.0057 ± 0.0005 [field 3506.5 ± 1.0]

g_2 = 2.0492 ± 0.0005 [field 3430.7 ± 1.0]

g_3 = 2.0684 ± 0.0005 [field 3399.2 ± 1.0]

These 3 values are typical of organic radical species but cannot be interpreted any further as the degradation products of the dye are not known precisely. To gain additional mechanistic information, EPR experiments were carried out on carmine red in solution in tert-butylbenzene.

In a first experiment, carminic acid was mixed with diphenyl iodonium hexafluorophosphate (DPI), well known for its oxidazing properties i.e. DPI is an excellent electron acceptor to simulate the photooxidation of the dye upon light irradiation. In a second one, the dye was mixed with ethyl dimethylamino benzoate (EDB), a chemical compound with a reducing properties (amines are good electron donors) to simulate photoreduction of the dye upon irradiation.

In both experiments, spin trap, N-tert-Butyl-α-phenylnitrone (PBN) was added, to ensure detection of any formed radical after mixing, or during photo-activation.

Figure 15 present the EPR spectra corresponding to these two experiments.

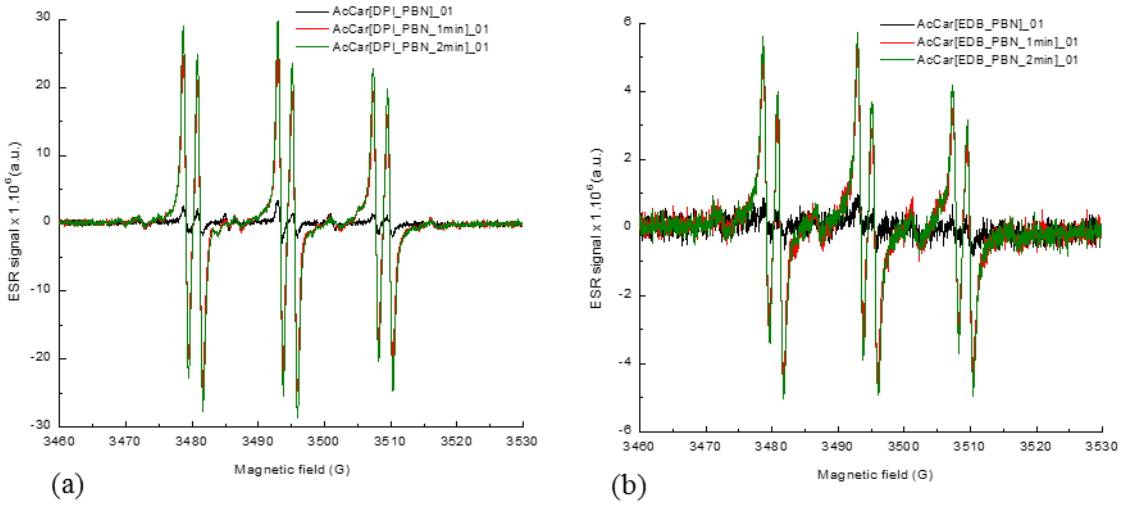

Figure 15: EPR of Carminic Acid with a) DPI and with b) EDB

In both cases, a clear effect is observed, which shows that carminic acid can behave both as an oxidant and a reducing agent. upon light irradiation. The oxidation and reduction potentials of carminic acid were determined as 1.32V and -0.88V, respectively. These potentials being also typical of rather good electron donor and acceptor in agreement with potential photooxidation or photoreduction of carminic acid upon light.

Conclusion

The first question that may be asked is what happens initially when the cationic polymer-clay composite is in contact with carminic acid. In the composite, as shown by XRD and TEM experiments, the cationic polymer appears to be at least partially intercalated in the interlayer clay space since the d001 values obtained for both hydrated and dehydrated systems are higher in the presence of polymers. Furthermore, DFT calculations confirm the intercalation of cationic polymers in the hydrated interlayer space of Mt. In such conditions, carminic acid is very unlikely to be able to access the interlayer space. When high amounts of cationic polymer are contacted with montmorillonite, charge inversion is observed through excess

adsorption of cationic polymers, which can provide a favourable environment for carminic acid adsorption. Dye adsorption indeed occurs in such conditions as revealed by both IR and NMR spectroscopy. The main adsorption mechanism appears to be hydrogen bonding between OH groups of the carminic acid and both surface groups present on the edge faces of clay mineral and adsorbed cationic polymers molecules present on basal faces.

The DFT calculations highlighted the role of water in the stabilization of CA on Mt surface. via hydrogen bonds.

Consequently, as the interactions between dye molecules and CP-Mt composites are mainly of van der Waals type, dye photostability in such composite is only marginally improved as revealed by irradiation experiments. Still, hydrogen bonding prevents the release of dye molecules when the composites are placed in various solvents. Such a feature may be advantageously used to design environmental applications (depollution) of clay-polymer composites. Finally, EPR results clearly show that photodegradation involves the formation of organic radicals the amount of which increases with irradiation time. Further experiments would be required to precisely unravel these degradation mechanisms via a radicalar approach.

Acknowledgements:

HPC resources from GENCI-[CCRT/CINES/IDRIS] (Grant 2016-[x2016082022]) and the CCRE of Université Pierre et Marie Curie are also acknowledged

References

[1] S. Garfield, Mauve: how one man invented a color that changed the world.; , Company, NY., , 2002.

[2] A. Gürses, M. Açıkyıldız, K. Güneş, M.S. Gürses, Dyes and pigments, SpringerBriefs in Green Chemistry for Sustainability ed., 2016.

[3] F.A. Aeschlimann, B.A. Michel, A.G. Aeschlimann, Pierre Auguste Renoir (1841-1919) "The Pain goes away, the Beauty remains", Aktuelle Rheumatol., 41 (2016) 440-441.

[4] S. Jamikorn, S. Vivekaphirat, V. Somsongkul, W. Suanthaisong, A. Naikaew, A. Wongchaisuwat, M. Arunchaiya, Dye-sensitized Solar Cell Based on Composite Poly(ethylene oxide) Electrolyte with Natural Carmine Pigment, Chiang Mai Journal of Science, 43 (2016) 1113-1121.

[5] O. Martinez-Zapata, J. Mendez-Vivar, P. Bosch, V.H. Lara, Synthesis and characterization of amorphous aluminosilicates prepared by sol-gel to encapsulate organic dyes, Journal of Non-Crystalline Solids, 357 (2011) 3480-3485.
[6] O. Martinez-Zapata, J. Mendez-Vivar, P. Bosch, V.H. Lara, Trapping organic molecules in sol-gel aluminosilicate matrices, Journal of Non-Crystalline Solids, 355 (2009) 2496-2502.
[7] E. Perez, I.A. Ibarra, A. Guzman, E. Lima, Hybrid pigments resulting from several guest dyes onto gamma-alumina host: A spectroscopic analysis, Spectrochimica Acta Part a-Molecular and Biomolecular Spectroscopy, 172 (2017) 174-181.
[8] F. Fournier, L. de Viguerie, S. Balme, J.M. Janot, P. Walter, M. Jaber, Physico-chemical characterization of lake pigments based on montmorillonite and carminic acid, Applied Clay Science, 130 (2016) 12-17.
[9] F.A.R. Pereira, K.S. Sousa, G.R.S. Cavalcanti, D.B. Franca, L.N.F. Queiroga, I.M.G. Santos, M.G. Fonseca, M. Jaber, Green biosorbents based on chitosan-montmorillonite beads for anionic dye removal, Journal of Environmental Chemical Engineering, 5 (2017) 3309-3318.
[10] M. Jaber, J. Miehe-Brendle, R. Le Dred, Mercaptopropyl Al-Mg phyllosilicate: Synthesis and characterization by XRD, IR, and NMR, Chemistry Letters, (2002) 954-955.
[11] J. Bujdak, N. Iyi, Molecular aggregation of rhodamine dyes in dispersions of layered silicates: Influence of dye molecular structure and silicate properties, Journal of Physical Chemistry B, 110 (2006) 2180-2186.
[12] T. Baranyaiova, J. Bujdak, Reaction kinetics of molecular aggregation of rhodamine 123 in colloids with synthetic saponite nanoparticles, Applied Clay Science, 134 (2016) 103-109.
[13] J. Bujdak, Hybrid systems based on organic dyes and clay minerals: Fundamentals and potential applications, Clay Minerals, 50 (2015) 549-571.
[14] J. Bujdak, J. Ratulovska, A. Donauerova, H. Bujdakova, Hybrid Materials Based on Luminescent Alkaloid Berberine and Saponite, Journal of Nanoscience and Nanotechnology, 16 (2016) 7801-7804.
[15] T. Endo, N. Nakada, T. Sato, M. Shimada, FLUORESCENCE OF CLAY-INTERCALATED XANTHENE DYES, Journal of Physics and Chemistry of Solids, 49 (1988) 1423-1428.
[16] T. Endo, N. Nakada, T. Sato, M. Shimada, THE FLUORESCENCE PROPERTIES OF COUMARINE DYE INTERCALATED IN A SWELLING CLAY, Journal of Physics and Chemistry of Solids, 50 (1989) 133-137.
[17] T. Saito, K. Fukui, Y. Kodera, A. Matsushima, H. Nishimura, Y. Inada, Photostability of biliverdin bound to smectite, clay mineral, Dyes and Pigments, 65 (2005) 21-24.
[18] F. Sanchez-Ochoa, G.H. Cocoletzi, G. Canto, Trapping and diffusion of organic dyes inside of palygorskite clay: The ancient Maya Blue pigment, Microporous and Mesoporous Materials, 249 (2017) 111-117.
[19] S. Gaweda, G. Stochel, K. Szacilowski, Photosensitization and Photocurrent Switching in Carminic Acid/Titanium Dioxide Hybrid Material, Journal of Physical Chemistry C, 112 (2008) 19131-19141.
[20] K. Jorgensen, L.H. Skibsted, Light Sensitivity of Cochineal. Quantum Yields for Photodegradation of Carminic Acid and Conjugate Bases in Aqueous Solution, Food Chemistry, 40 (1991) 25-34.
[21] Y.H. Chen, S.J. Huang, B.Z. Wan, Reversal of Zeta Potential of Proton-Type Zeolite Y after Surface Modifications in Sodium Ion Aqueous Solutions, Industrial & Engineering Chemistry Research, 55 (2016) 1921-1928.
[22] H.P. Chao, S.H. Chen, Adsorption characteristics of both cationic and oxyanionic metal ions on hexadecyltrimethylammonium bromide-modified NaY zeolite, Chemical Engineering Journal, 193 (2012) 283-289.
[23] K. Barquist, S.C. Larsen, Chromate adsorption on amine-functionalized nanocrystalline silicalite-1, Microporous and Mesoporous Materials, 116 (2008) 365-369.
[24] C. Breen, R. Watson, Polycation-exchanged clays as sorbents for organic pollutants: Influence of layer charge on pollutant sorption capacity, Journal of Colloid and Interface Science, 208 (1998) 422-429.
[25] G.J. Churchman, Formation of complexes between bentonite and different cationic polyelectrolytes and their use as sorbents for non-ionic and anionic pollutants, Applied Clay Science, 21 (2002) 177-189.

[26] E.R. Ruiz-Hitzky, M. Darder, P. Aranda, Functional biopolymer nanocomposites based on layered solids, Journal of Materials Chemistry, 15 (2005) 3650-3662.
[27] M. Jaber, T. Georgelin, H. Bazzi, F. Costa-Torro, J.F. Lambert, G. Bolbach, G. Clodic, Selectivities in Adsorption and Peptidic Condensation in the (Arginine and Glutamic Acid)/Montmorillonite Clay System, Journal of Physical Chemistry C, 118 (2014) 25447-25455.
[28] M. Jaber, J. Miehe-Brendle, Influence of the synthesis medium on the saponite crystallisation: formation mechanism in acidic and basic media, Comptes Rendus Chimie, 8 (2005) 229-234.
[29] S.B. Zeskoski, Historical Pigments and the Role of Alchemy in their Production: an Interdisciplinary Study, Portal-Godisnjak Hrvatskog Restauratorskog Zavoda, (2017) 21-41.
[30] S. Kroustallis, Cennino Cennini's Il Libro dell'Arte: A new English translation and commentary with Italian transcription, Ge-Conservacion, (2016) 128-130.
[31] F. Frezzato, CENNINO CENNINI'S IL LIBRO DELL'ARTE. A NEW ENGLISH TRANSLATION AND COMMENTARY WITH ITALIAN TRANSCRIPTION, Journal of the American Institute for Conservation, 55 (2016) 186-188.
[32] S. Balme, J.-M. Janot, P. Déjardin, P. Seta, Highly efficient fluorescent label unquenched by protein interaction to probe the avidin rotational motion, Journal of Photochemistry and Photobiology A: Chemistry, 184 (2006) 204-211.
[33] D.V. O'Connor, D. Phillips, Time Correlated Single Photon Counting, Academic Press, New-York, 1984.
[34] G. Kresse, J. Hafner, ABINITIO MOLECULAR-DYNAMICS FOR LIQUID-METALS, Physical Review B, 47 (1993) 558-561.
[35] G. Kresse, J. Hafner, AB-INITIO MOLECULAR-DYNAMICS SIMULATION OF THE LIQUID-METAL AMORPHOUS-SEMICONDUCTOR TRANSITION IN GERMANIUM, Physical Review B, 49 (1994) 14251-14269.
[36] J.P. Perdew, K. Burke, M. Ernzerhof, Generalized gradient approximation made simple, Physical Review Letters, 77 (1996) 3865-3868.
[37] J.P. Perdew, K. Burke, M. Ernzerhof, Generalized gradient approximation made simple (vol 77, pg 3865, 1996), Physical Review Letters, 78 (1997) 1396-1396.
[38] K. El Adraa, T. Georgelin, J.F. Lambert, F. Jaber, F. Tielens, M. Jaber, Cysteine-montmorillonite composites for heavy metal cation complexation: A combined experimental and theoretical study, Chemical Engineering Journal, 314 (2017) 406-417.
[39] M. Bouchoucha, F. Tielens, F. Gaslain, F. CostaTorro, S. Casale, A. Palcic, V. Valtchev, J.F. Lambert, M. Jaber, Melanin Polymerization Held in Check: A Composite of Dihydroxyphenylalanine with Zeolite Beta, Journal of Physical Chemistry C, 119 (2015) 8736-8747.
[40] K. El Adraa, V. Timon, J.F. Lambert, A.R. Al-Rabaa, F. Jaber, M. Jaber, F. Tielens, Adsorption of L-DOPA Intercalated in Hydrated Na-Saponite Clay: A Combined Experimental and Theoretical Study, Journal of Physical Chemistry C, 116 (2012) 26414-26421.
[41] P. Margl, K. Schwarz, P.E. Blochl, FINITE-TEMPERATURE CHARACTERIZATION OF FERROCENE FROM FIRST-PRINCIPLES MOLECULAR-DYNAMICS SIMULATIONS, Journal of Chemical Physics, 100 (1994) 8194-8203.
[42] S. Grimme, Semiempirical GGA-type density functional constructed with a long-range dispersion correction, Journal of Computational Chemistry, 27 (2006) 1787-1799.
[43] M. Dion, H. Rydberg, E. Schroder, D.C. Langreth, B.I. Lundqvist, Van der waals density functional for general geometries (vol 92, art no 246401, 2004), Physical Review Letters, 95 (2005).
[44] M. Lepoitevin, M. Jaber, R. Guegan, J.-M. Janot, P. Dejardin, F. Henn, S. Balme, BSA and lysozyme adsorption on homoionic montmorillonite: Influence of the interlayer cation, Applied Clay Science, 95 (2014) 396-402.
[45] D. Costa, A. Tougerti, F. Tielens, C. Gervais, L. Stievano, J.F. Lambert, DFT study of the adsorption of microsolvated glycine on a hydrophilic amorphous silica surface, Physical Chemistry Chemical Physics, 10 (2008) 6360-6368.
[46] N. Folliet, C. Roiland, S. Begu, A. Aubert, T. Mineva, A. Goursot, K. Selvaraj, L. Duma, F. Tielens, F. Mauri, G. Laurent, C. Bonhomme, C. Gervais, F. Babonneau, T. Azais, Investigation of the interface in

silica-encapsulated liposomes by combining solid state NMR and first principles calculations, Journal of the American Chemical Society, 133 (2011) 16815-16827.
[47] N. Folliet, C. Gervais, D. Costa, G. Laurent, F. Babonneau, L. Stievano, J.F. Lambert, F. Tielens, A Molecular Picture of the Adsorption of Glycine in Mesoporous Silica through NMR Experiments Combined with DFT-D Calculations, Journal of Physical Chemistry C, 117 (2013) 4104-4114.
[48] A. Cimas, F. Tielens, M. Sulpizi, M.-P. Gaigeot, D. Costa, The amorphous silica-liquid water interface studied by ab initio molecular dynamics (AIMD): local organization in global disorder, Journal of Physics-Condensed Matter, 26 (2014).
[49] J. Coates, J. Reffner, Have FT-IR ... Will travel, Spectroscopy, 15 (2000) 19-29.
[50] M.C. Rosu, R.C. Suciu, M. Mihet, I. Bratu, Physical-chemical characterization of titanium dioxide layers sensitized with the natural dyes carmine and morin, Mater. Sci. Semicond. Proc. , 16 (2013) 1551–1557.
[51] A.P. Periasamy, Y.H. Ho, S.M. Chen, Multiwalled carbon nanotubes dispersed in carminic acid for the development of catalase based biosensor for selective amperometric determination of H2O2 and iodate, Biosens. Bioelectron. , 29 (2011) 151–158.
[52] Y. Kohno, K. Totsuka, S. Ikoma, K. Yoda, M. Shibata, R. Matsushima, Y. Tomita, Y. Maeda, K. Kobayashi, Photostability enhancement of anionic natural dye by intercalation into hydrotalcite, Journal of Colloid and Interface Science, 337 (2009) 117-121.
[53] S. Balme, R. Guegan, J.-M. Janot, M. Jaber, M. Lepoitevin, P. Dejardin, X. Bourrat, M. Motelica-Heino, Structure, orientation and stability of lysozyme confined in layered materials, Soft Matter, 9 (2013) 3188-3196.
[54] V. Tangaraj, J.M. Janot, M. Jaber, M. Bechelany, S. Balme, Adsorption and photophysical properties of fluorescent dyes over montmorillonite and saponite modified by surfactant, Chemosphere, 184 (2017) 1355-1361.